Recent Progress in Fabrication of Hollow Nanostructures

Ryusuke Nakamura and Hideo Nakajima

Abstract Hollow nanostructures are of great interest in many current and emerging areas of technology. In the last few years, a variety of ideas to fabricate hollow nanostructures (e.g., hollow nanospheres, nanoboxes, nanocages, and nanotubes) have been proposed. This review work covers several typical methods to fabricate hollow nanoparticles and nanotubes. The methods introduced in this article are categorized into two parts: one is based on the chemical synthesis routes including conventional templating-etching and galvanic replacement and the other is based on the Kirkendall effect, which is a diffusional phenomena at the solid–solid interface. Furthermore, structural stability of hollow nanoparticles and nanotubes during annealing at high temperatures is discussed.

1 Introduction

In recent years, considerable effort has been put into the design and fabrication of nanostructured materials with functional properties (e.g., nanoparticles, nanorods, etc.) [1]. Above all, it is important to obtain nanostructures with a specific size and morphology, taking into consideration their specific applications. Therefore, the control of the shape of nanoparticles and nanowires is one of the most important topics in the current research on nanomaterials. In particular, there is an increasing

R. Nakamura (✉) and H. Nakajima
The Institute of Scientific and Industrial Research, Osaka University,
Mihogaoka 8-1, Ibaraki, Osaka 567-0047, Japan
e-mail: rnakamur@sanken.osaka-u.ac.jp

H. Nakajima
e-mail: nakajima@sanken.osaka-u.ac.jp

Adv Struct Mater (2013) 4: 3–30
DOI: 10.1007/8611_2010_42

Published Online: 17 November 2010

interest in methods to fabricate hollow nanostructures because their unique shape makes them applicable as delivery vehicles, fillers as well as for catalysis, and is expected to bring about changes in chemical, physical, and catalytic properties. The recent progress in synthesis and applications of hollow nanoparticles and nantoubes has been already reviewed by Xia et al.[2], Fan et al. [3], Lou et al. [4], and An and Hyeon [5].

In general, the most popular concept of methods to fabricate hollow nanostructures can be recognized as the combination of templating, coating and chemical etching. By coating the surface of the template nanoparticles or nanowires and removing the template by chemical etching, a wide variety of materials with hollow structures have been successfully synthesized. Meanwhile, the other types of methods based on self-organization have become available; the specific phenomena such as the Kirkendall effect [6] and Ostwald ripening [7] have been applied to the fabrication of hollow nanostructures. Since Yin et al. [8] published the results of the synthesis of hollow nanoparticles using the Kirkendall effect, which is a diffusional phenomenon at the interface between different solids, in 2004, the number of reports are increasing up to now.

In this review, we will overview the recent progress on the fabrication of hollow nanostructures: first the reports based on chemical synthesis routes and next on the Kirkendall effect. In the last section, our latest studies on the structural stability of hollow nanoparticles and nanotubes at high temperatures will be introduced in detail.

2 Fabrication Routes to Hollow Nanostructures

2.1 Techniques Based on Chemical Routes

The combination of templating and etching is a conventional route to fabricating hollow nanostructures. In general, it involves the four steps illustrated in Fig. 1 [4] (1) preparation of hard templates (usually polymer or silica); (2) functionalization/

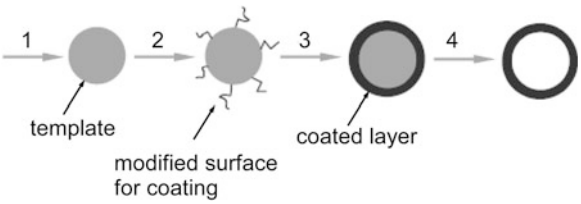

Fig. 1 Schematic illustration of a conventional hard templating process for hollow sphere synthesis. (*1*) preparation of hard templates such as polymer and silica, (*2*) modification of template surface, (*3*) coating the templates with designed materials, and (*4*) removal of templates and formation of hollow structures (reproduced with permission from [4])

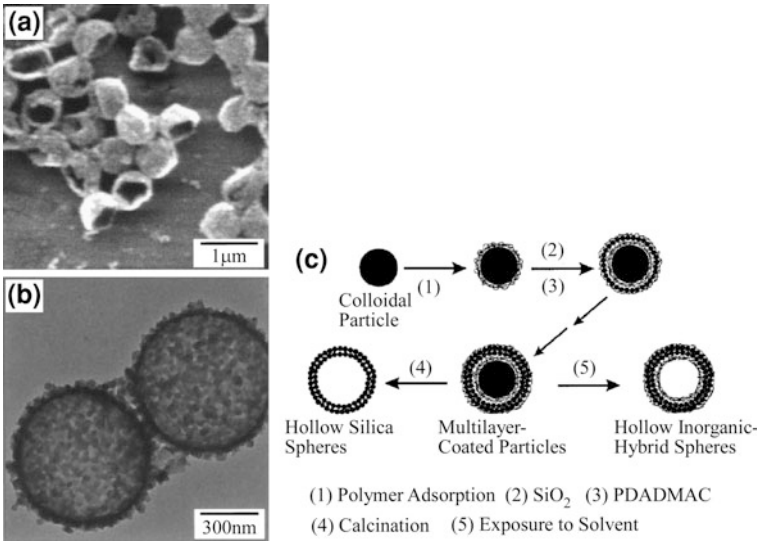

Fig. 2 **a** SEM and **b** TEM micrographs of hollow silica spheres produced by calcination of PS(Polystyrene) latices coated with one SiO_2-PDADMAC(poly-di-allyl-dimethyl-ammonium-chloride) multilayer. Both broken and intact hollow spheres were observed in these samples. The uniformity of the wall thickness can be seen in **b**. **c** Illustration of procedures for preparing inorganic and hybrid hollow spheres (reproduced with permission from [9])

modification of templated surface to achieve favorable surface properties; (3) coating the templates with designed materials or their precursors by various approaches; and (4) selective removal of the templates to obtain hollow nanostructures. Figures 2 and 3 show examples of hollow SiO_2 [9] and Pd [10] on the basis of the templating and etching methods, respectively. For example, the synthesis process of hollow Pd is as follows: (1) The uniform silica spheres were synthesized, (2) the surfaces of the silica spheres were functionalized with mercaptopropylsilyl (MPS) groups by refluxing the silica spheres and mercaptopropyltrimethoxysilane ($HS(CH_2)_3$-$Si(OCH_3)_3$) in toluene, (3) the palladium precursor, palladium acetylacetonate ($Pd(acac)_2$), was adsorbed onto the surfaces of these MPS-functionalized silica spheres and were then heated at 250°C for 3 h to obtain Pd metal-coated spheres, and finally (4) the silica template was removed by treating the Pd-coated silica spheres with 10 M HF. The technique has also been extensively applied to obtain hollow nanoparticles of a wide range of inorganic materials, including TiO_2 [11, 12], SnO_2 [13], Au [14], Fe_3O_4 [15]. Another examples are reviewed by Lou et al. [4], who categorized the conventional hard templating methods into six groups according to coating process. Furthermore, Lou et al. [4] summarized soft-template methods using liquid and gaseous templates against hard templates using solid materials.

The disadvantage of the template-mediated methods were pointed out by An and Heyon [5]; (1) the hollow nanostructures obtained via a template-mediated

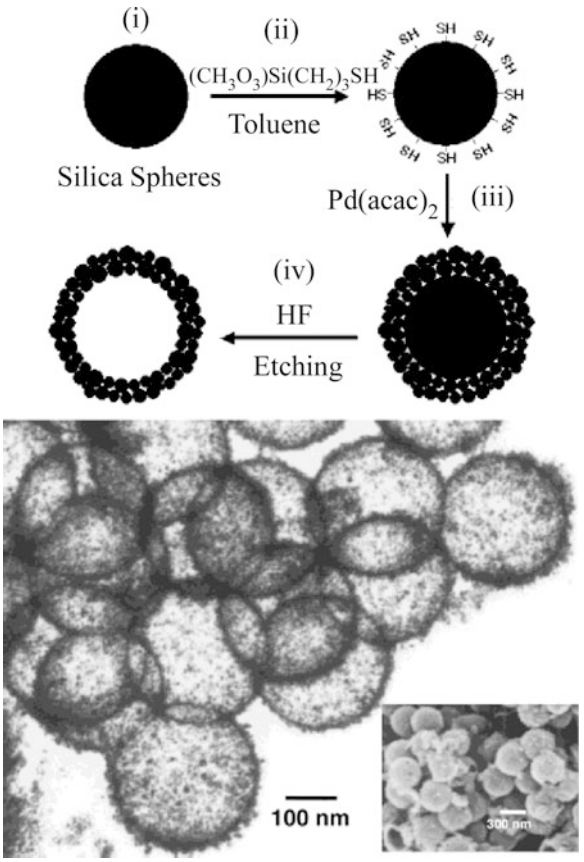

Fig. 3 Transmission electron micrograph and scanning electron micrograph (*inset*) of hollow palladium spheres and illustration of synthesis process: (*i*) preparation of uniform silica spheres, (*ii*) the functionalization of the surfaces of the silica spheres with mercaptopropylsilyl (MPS) and mercaptopropyl-trimethoxysilane ($HS(CH_2)_3$-$Si(OCH_3)_3$) in toluene, (*iii*) adsorption of the palladium precursor, palladium acetylacetonate ($Pd(acac)_2$) onto the surfaces of these MPS-functionalized silica spheresand and heating at 250°C for 3 h to obtain Pd metal-coated spheres, and finally (*iv*) removal of the silica template by treating the Pd-coated silica spheres with 10 M HF (reproduced with permission from [10])

route using silica or polymer particles as the templates are often larger than 200 nm because it is hard to make smaller template particles and (2) the post-treatment necessary to remove the templates adds complexity to the whole synthetic process and increases the chance of the structural deformation as well as the introduction of impurities.

This idea is also useful for fabricating nanotube structures. For example, GaN nanotubes were fabricated through the preparation of ZnO/GaN core/shell structures and the subsequent removal of ZnO nanowires, as shown in Fig. 4 [16]. The arrays of ZnO nanowires were grown on (110) sapphire wafers using a vapor deposition process and then GaN chemical vapor was deposited epitaxially on the ZnO nanowire arrays placed inside a reaction tube. The core part of ZnO can be removed from ZnO/GaN wires by chemical etching with ammonia at high temperature or thermal reduction at high temperatures (for example, 873 K in H_2). The synthesis of Zn_3P_2, Cd_3P_2 [17] and Al_2O_3 [18] nanotubes based on templating and etching method were also reported.

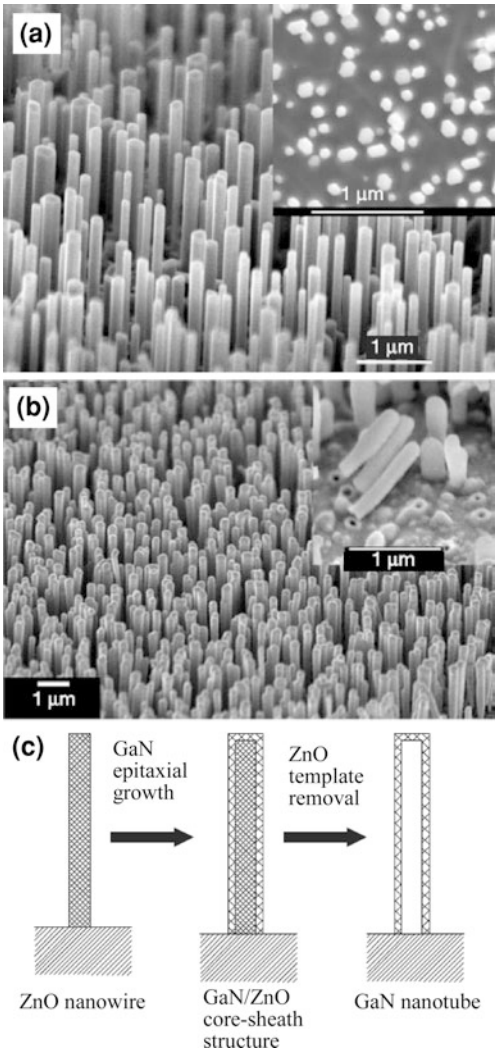

Fig. 4 Arrays of ZnO nanowires and GaN nanotubes. Shown are SEM images of the ZnO nanowire template arrays (**a**), and the resulting GaN nanotube array (**b**). *Inset* in **a** shows cross-sections of the ZnO nanowires. *Inset* in **b** shows the fractured interface between the GaN nanotubes and the substrate. **c** Schematic illustration of the 'epitaxial casting' process for making single-crystal GaN nanotubes (reproduced with permission from [16])

Schmidt and Eberl [19, 20] showed that layered Si-Ge rolled up to form nanoscrolls by strain release of the lattice-mismatched film-substrate interface. Figure 5 shows illustrations of the mechanisms and the obtained nanotubes according to the mechanisms: (a) General method to create a nanotube (method I). An etchant-sensitive material is deposited on a substrate surface. On top of this substrate, a thin film (or a series of thin films) is deposited. After selective etching of the substrate, the thin top layer is wrapped up and folded back onto the sample surface, where it can bond to itself. At the position where the layer bends, a nanotube has formed. (b) Specialized way to create a nanotube (method II). The layer sequence consists of an etchant-sensitive material, followed by a bilayer of

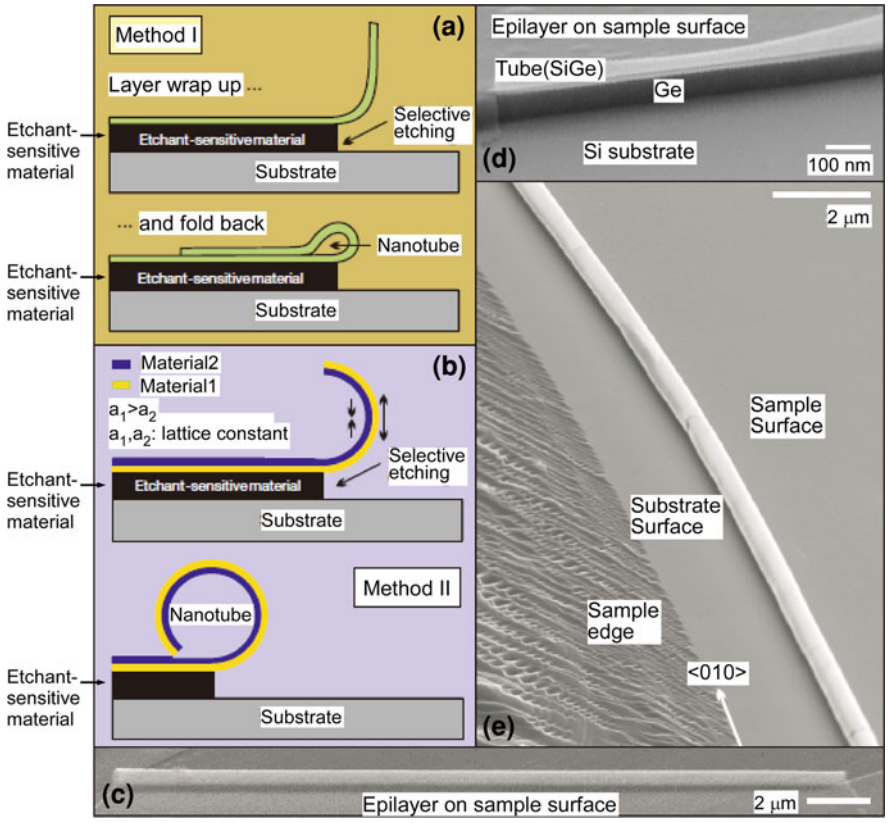

Fig. 5 Formation of solid-state nanotubes. **a** General method to create a nanotube (method I). **b** Specialized way to create a nanotube (method II). **c**, **d** Folded nanotubes fabricated according to method I. 'Epi' layer indicates epitaxial layer. **e** SiGe-based nanotube formed along the edge of a sample (by method II) (reproduced with permission from [19])

two different materials (materials 1 and 2). Material 1 has a larger lattice constant than material 2, so $a_1 > a_2$. Once the bilayer is released by selective etching, each material tends to acquire its inherent lattice constant. The bilayer bends upwards, finally forming a nanotube after one complete revolution. Longer etching times result in multiple revolutions. (c, d) Folded nanotubes fabricated according to method I. 'Epi' layer indicates epitaxial layer. (e) SiGe-based nanotube formed along the edge of a sample (by method II). Although this technique is based on the combination of templating and etching, the process of rolling up is different from the typical templating methods introduced above.

The galvanic replacement reaction has been applied for the synthesis of hollow nanostructures of novel metals such as Au, Pt and Pd. In the synthetic process for hollow Au nanoboxes or frames, for example, $HAuCl_4$ is added to the suspension of Ag nanocubes with the amount of $HAuCl_4$ and reaction temperature

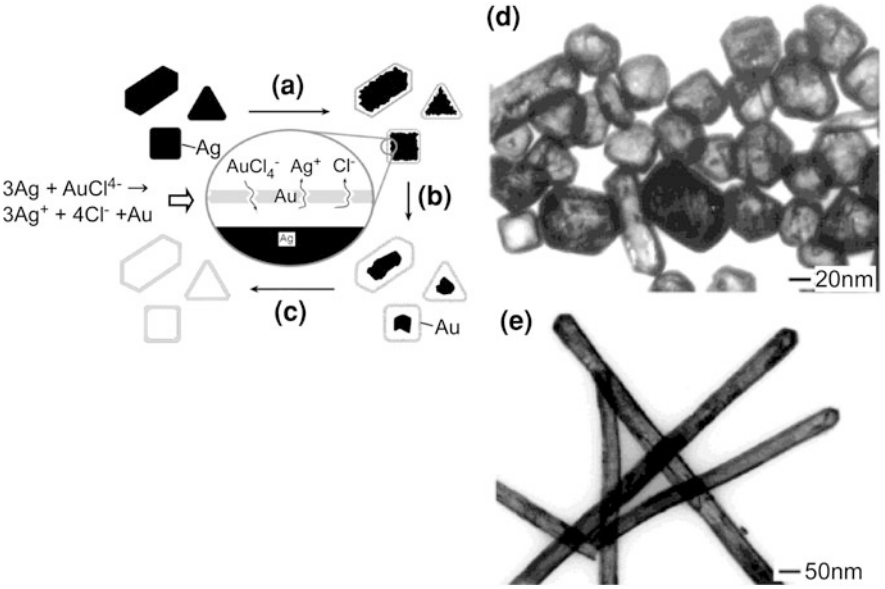

Fig. 6 Schematic illustration of the experimental procedure that generates nanoscale shells of gold from silver templates with various morphologies. The reaction is illustrated in the schematic as follows: **a** Addition of $HAuCl_4$ to a dispersion of silver nanoparticles and initiation of the replacement reaction; **b** The continued replacement reaction of $HAuCl_4$ with the silver nanoparticles; **c** Depletion of silver and annealing of the resultant shells to generate smooth hollow structures. **d**, **e** TEM image of gold nanoshells and nanotubes formed by reacting these silver nanoparticles with an aqueous $HAuCl_4$ solution (reproduced with permission from [21])

being controlled. The silver template-mediated galvanic replacement reaction is described as follows:

$$3Ag(s) + AuCl_4^-(aq) \rightarrow Au(s) + 3Ag^+(aq) + 4Cl^-(aq)$$

In the reaction, Ag nanoparticles act as a template. SEM images of the formation of Au nanoboxes and nanocages using the above reaction are shown in Fig. 6 [21]. According to the amount of $HAuCl_4$, the nanostructures develop; Au/Ag nanoboxes interior nanoholes → Au nanoboxes with uniform wall thickness → Au nanoframes with porous walls. Similarly, Pt/Ag and Pd/Ag hollow nanostructures have been prepared via the galvanic replacement because both $PtCl_4^-$ and $PdCl_4^{2-}$ ions have higher standard reduction potential than AgCl/Ag pair [22]. It has been pointed out that despite the simplicity of the chemistry, the formation mechanism of hollow structures via the galvanic replacement can be complicated, depending on the reaction system [23].

Finally, an example of template-free methods is introduced. Recently, one-step self-templated methods based on Ostwald ripening have been applied to synthesize hollow structures. Ostwald ripening, first described by Ostwald in 1896 [7], is a spontaneous process which refers to the growth of large precipitates at the expense

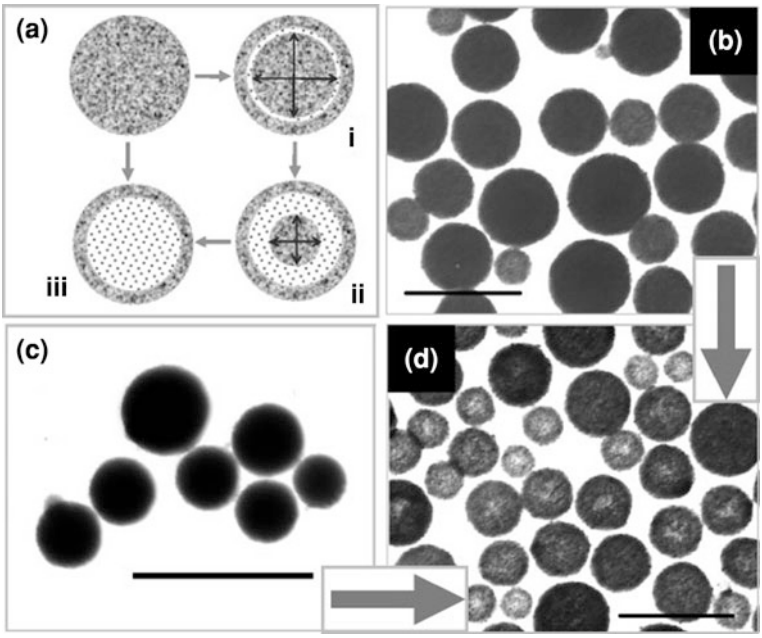

Fig. 7 **a** Schematic illustration (cross-sectional views) of the proposed inside-out ripening mechanism: inside-out evacuation can initiate from just below the surface to form particle (*i*) then evolve to core/shell particle (*ii*), and possibly to hollow particle *iii*, or start around the central region of the solid spheres and evolve to particle (*iii*) directly. **b** Typical TEM image of SnO_2 nanospheres obtained with 6 h reaction at 150°C (r = 37.5%, c = 14.0 mM, 0.1 M urea). **c** Typical TEM image of amorphous SnO_2 nanospheres obtained by aging the reaction mixture (r = 37.5%, c = 14.0 mM, 0.1 M urea) for several days at room temperature. D) Typical TEM image of SnO_2 hollow nanospheres synthesized at 150°C for 24 h with the reaction mixture (r = 37.5%, c = 14.0 mM, 0.1 M urea) aged for several days (corresponding to **c**) or without aging (18 h further reaction based on **b**). All three *scale bars* 500 nm (reproduced with permission from [24])

of smaller precipitates caused by energetic factors. Lou et al. [24] reported a simple one-pot template-free synthesis of polycrystalline SnO_2 hollow nanostructures, as shown in Fig. 7. At the initial stage of reaction, amorphous solid nanospheres are formed by hydrolyzation of stannate. With time, the surface layer of the nanospheres crystallizes first due to contact with surrounding solution. As a result, the materials inside the solids spheres have a strong tendency to dissolve, which provides the driving force for the spontaneous inside-out Ostwald ripening. Although fundamental evidence in support of this mechanism is not enough, it has been shown to be applicable in many systems, including TiO_2 [25], Cu_2O [26], ZnS and Co_3O_4 [27], etc. These hollow materials were synthesized through chemical reaction processes. Therefore, they have been introduced in this section although Ostwald ripening itself is not defined as a chemical reaction.

2.2 Kirkendall-Effect-Related Methods

2.2.1 Hollow Nanoparticles

Kirkendall effect as a classical phenomenon in metallurgy was established [6]. It basically refers to a nonreciprocal mutual diffusion process through an interface of two metals so that vacancy diffusion occurs to compensate for the unequality of the mass flow and that the initial interface moves. Smigelskas and Kirkendall observed a movement of the initial interface in a Cu/brass diffusion couple, as a result of a faster diffusion of zinc into the copper than that of copper into the brass (the intrinsic diffusion coefficient of Zn is 2.5 times as large as that of Cu at 785°C.) The Kirkendall experiment demonstrated two important facts: (1) atomic diffusion occurs via vacancies and (2) each metal diffuses at a different mobility. In some cases, condensation of excess vacancies can give rise to void formation, called 'Kirkendall voids', near original interface and within the faster diffusion side.

Formation of the Kirkendall voids is basically unfavorable from the viewpoint of technological application. Engineers try to avoid this effect in the case that interdiffusion occurs at the bonded-interface because the Kirkendall voids deteriorate the bonding strength of the bond-pad interface or may cause wire bond failure in integrated circuits. On the other hand, chemists applied the destructive effect constructively for synthesizing hollow nanostructures in a way that the Kirkendall voids coalesce into a single hollow core. Yin et al. [8] demonstrated that initially solid Co nanoparticles transformed into hollow nanoparticles through the reaction with sulfur, oxygen and selenium. An example of hollow cobalt sulfides is shown in Fig. 8. The sulfidation of cobalt nanoparticles resulted in the formation of hollow cobalt sulfide of either Co_3S_4 or Co_8S_9, depending on the molar ration of sulfur and cobalt. During the reaction, the surfaces of cobalt nanoparticles are covered with the sulfide layers and the diffusion of cobalt and sulfur atoms in opposite direction occurs through the sulfide layers. As the reaction proceeds, voids are formed in the cobalt side of the interface because the outward diffusion of cobalt ions is much faster than the inward diffusion of sulfur.

Their work has inspired a number of studies that attempt to apply the nanoscale Kirkendall effect to create hollow nanostructures [28–56]. Nanoscale hollow structures by a route related to the Kirkednall effect are listed in Table 1, where some reports published after 2007 were added to the original list given by Fan et al. [3]. Particularly, hollow oxide formation via oxidation of metal nanoparticles was investigated relatively for many metals such as Al, Cu [31], Fe [41–44], Ni [46] and Zn [52–54]. Nakamura et al. [31] demonstrated that a reaction of Pb nanoparticles with oxygen resulted in the formation of solid PbO because the diffusivity of oxygen is known to be larger than that of Pb in PbO, suggesting that the faster outward diffusion of metal ions than inward diffusion of oxygen ions is essential for the formation of hollow oxides through oxidation reaction.

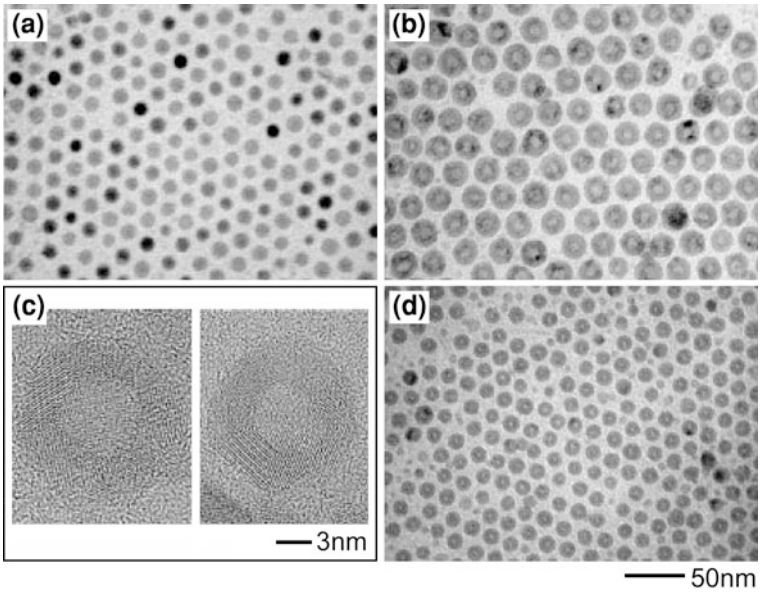

Fig. 8 **a** TEM image of cobalt nanocrystals synthesized by the injection of 0.54 g of $Co_2(CO)_8$ in 3 ml of o-dichlorobenzene into 0.1 ml of oleic acid and 0.1 g of trioctylphosphine oxide in 15 ml of *o*-dichlorobenzene at 182°C. **b** TEM image of the cobalt sulfide phase synthesized by the injection of sulfur in *o*-dichlorobenzene (5 ml) into cobalt nanocrystal solution with a Co/S molar ratio of 9:12. Co_3S_4 particles were synthesized from the cobalt sample shown in **a**. **c** HRTEM images of Co_3S_4 (*left*) and Co_9S_8 (*right*). **d** TEM image of the cobalt sulfide phase synthesized as in **b** (reproduced with permission from [8])

During the oxidation or sulfidation of metal nanoparticles, voids are formed at the interface. Tokozakura et al. [57] showed that voids formed at the interface retard the outward diffusion of remaining metals.

Formation of hollow oxide nanoparticles was found at low temperatures for Fe, Al and Zn. Nakamura et al. observed that in the case of smaller Zn (below 20 nm in diameter) and Al (below 8 nm in diameter) nanoparticles, the rapid outward migration of metal ions at the initial oxidation stages makes hollow oxide particles and that larger hollow oxide particles could not be formed by thermal oxidation at around 400 K. The fast outward diffusion of metal cations through the oxide layer is not thermally activated but driven by an electrical field built between the metal and an initial thin oxide layer according to the Cabrera–Mott theory. On the other hand, Cu nanoparticles were observed to turn into hollow Cu_2O regardless of initial diameter probably because the self-diffusion coefficient of Cu ions in Cu_2O at around 400 K is high enough to explain the growth of the Cu_2O layer via the thermal-activated diffusion process after the initial oxide formation.

Although hollow oxides with an almost uniform shell thickness were formed in the case of Co, Fe, Cu, and Al, a peculiar behavior of void formation during the oxidation of Ni nanoparticles can be seen [46]. In Fig. 9, the morphology change

Table 1 Hollow nanoparticles and nanotubes fabricated through the Kirkendall effect

Materials	Morphology	Ref.	Publication year
Ag_2Se	Nanotubes	[28]	2006
AlN	Hollow particles	[29]	2006
	Hollow particles	[30]	2007
Amorphous Al_2O_3	Hollow particles	[31]	2007
CdS	Polycrystal nanoshell	[32]	2005
Co_3S_4, CoO, CoSe	Hollow particles	[8]	2004
Co_3S_4	Porous nanowires	[33]	2006
	Nanotubes	[34]	2007
Co_3S_4, $CoSe_2$, CoTe	Hollow nanochains	[35]	2006
$CoSn_3$	Hollow nanorods	[36]	2008
Cu_2O	Hollow nanoparticles	[31]	2007
CuO	Hollow nanoparticles	[37]	2008
Cu_2O, CuO	Nanotubes	[38]	2009
CuS	Nanotubes	[39]	2007
Cu_7S_4	Nanocages	[40]	2005
Fe_xO_y	Hollow nanoparticles	[41]	2005
Fe_3O_4	Hollow nanoparticles	[42]	2007
γFe_2O_3	Hollow nanoparticles	[43]	2007
Fe_3O_4, γFe_2O_3	Hollow and porous nanoparticles and nanotubes	[44]	2009
MoS_2	Cubic microcages	[45]	2006
NiO	Hollow nanoparticles	[46]	2008
	Bamboo-like nanowires	[38]	2009
Ni_2P, Co_2P	Hollow nanoparticles	[47]	2007
SnO_2	Hollow nanoparticles	[48]	2008
PbS	Hollow nanoparticles	[49]	2005
$ZnAl_2O_4$	Nanotubes	[50, 51]	2006,2007
ZnO	Microcages	[52]	2004
	Dandelion	[53]	2004
	Hollow nanoparticles	[54]	2007
	Nanotubes	[55]	2008
$ZnSiO_4$	Nanotubes	[56]	2007

of Ni nanoparticles (1) after oxidation at 573 K for 7.2 ks and (2) at 673 K for 1.8 ks are shown. A single large void is formed at one off-center site of the interface between Ni and NiO (Fig. 9a) and hollow oxide nanoparticles with the nano-pores at localized position are formed (Fig. 9b). Although the formation mechanism of the nano-pore in NiO particles is similar with other hollow oxides such as Co-, Zn-, and Cu-oxides, hollow NiO has a peculiar morphology unlike them. The formation mechanism of a single localized void at the Ni/NiO interface during oxidation and an off-centered nano-pore in hollow NiO particles is discussed in terms of the atomic movement during oxidation. The growth behavior of the voids during the oxidation of Ni nanoparticles observed in Fig. 9a indicates that vacancies migrate toward a site of the interface and then become a large void at the site.

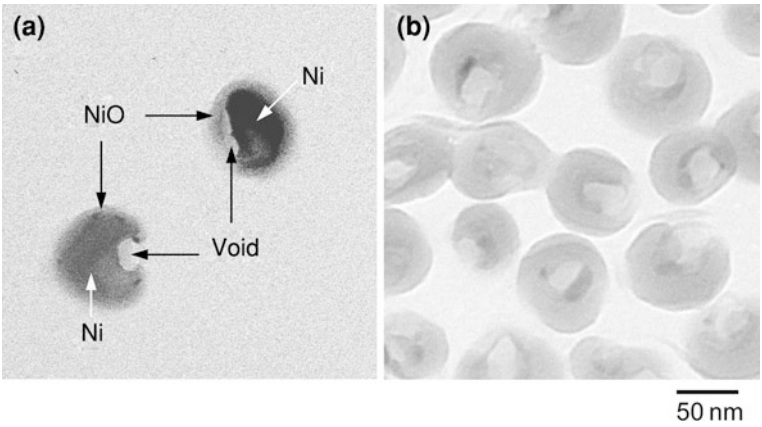

Fig. 9 TEM images of Ni nanoparticles after oxidation at **a** 300°C for 7.2 ks and **b** 400°C for 1.8 ks (reproduced with permission from [46])

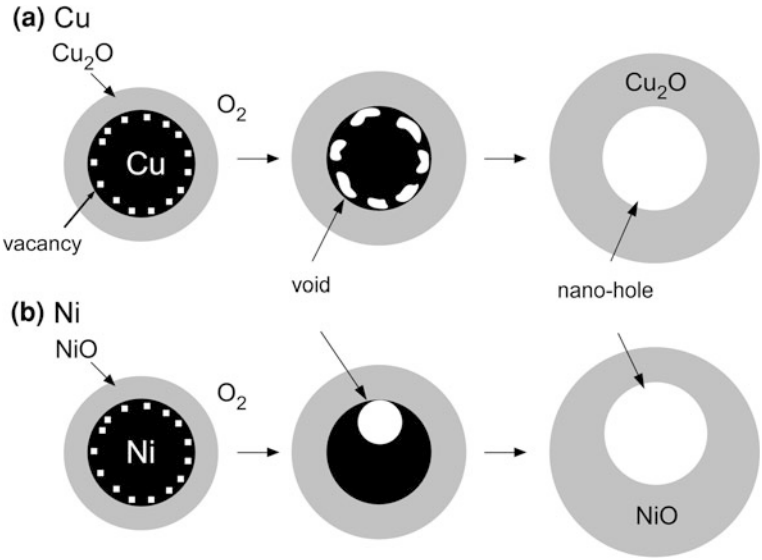

Fig. 10 Comparison of void formation behavior for oxidation of Cu nanoparticles with Ni nanoparticles (reproduced with permission from [46])

The formation of vacancies, voids and a nano-hole through the oxidation of Cu and Ni nanoparticles is illustrated in Fig. 10a, b, respectively. Vacancies are generated along the metal-side interface as a result of the outward diffusion of metal ions at the initial stage of oxidation. As oxidation proceeds, voids are formed uniformly along the Cu/Cu_2O interface by the clustering of neighboring vacancies (Fig. 10a), while they become large voids at one site on the Ni/NiO interface

(Fig. 10b) because of the long-range diffusion of vacancies. As a result, a nanohole is formed at the center part of Cu_2O particles, but it is off-centered in NiO particles. Vacancies generated in the oxidation process of Ni nanoparticles migrate to and aggregate at a site of the Ni/NiO interface since the mobility of vacancies inside Ni is large as the oxidation proceeds. This behavior can be interpreted as the self-assembly of vacancies and this allows an energetically more stable state to be achieved.

In general, the mechanism of metal sulfidation is known to be similar to that of metal oxidation. There are lots of reports on the formation of hollow sulfide nanoparticles such as Cu–S [39, 40], MoS_2 [45], and PbS [49].

2.2.2 Nanotubes

The Kirkendall effect has been extended to the fabrication of tubular structures. Fan et al. [50] demonstrated that $ZnAl_2O_4$ spinel nanotubes could be obtained using the Kirkendall effect. Figure 11 shows TEM images for the nanotubes together with the schematic illustrations of the formation process. As shown in the illustration, the starting material is a ZnO nanowire (10–30 nm thick, up to 20 μm long) coated by Al_2O_3 (10 nm thick). By annealing the core/shell nanowires, in air at 700°C for 3 h, a cylindrical interior nanopore is introduced during the solid-state diffusion between ZnO and Al_2O_3· ZnO/Al_2O_3 reaction is considered as a one-way transfer of ZnO into Al_2O_3 in a pseudo binary system. They pointed out that the conformity and uniformity of Al_2O_3 layers via atomic-layer-deposition are essential to the formation of smooth nanotubes. They reported that completely hollow $ZnAl_2O$ nanotubes could be obtained, whereas in the case of MgO/Al_2O_3, only porous $MgAl_2O_4$ nanowires were obtained without formation of complete nanotubes. They concluded that the difference in final morphology is attributed to that in crystal structure and diffusion of metal ions. Additionally, Fan et al. [51] showed the surface diffusion on the morphology evolution; the initial stage is the generation of small Kirkendall voids intersecting the compound interface via a bulk diffusion process, whereas the second stage is dominated by the surface diffusion of the core materials along the pore surface.

Another example of the formation of nanotubes through the Kirkendall effect is Ag_2Se [28]. TEM images of obtained Ag_2Se nanotubes are shown in Fig. 12, together with the schematic illustrations of the formation process. CSe_2 was first adsorbed onto the surfaces of the Ag nanowire templates, and subsequent photolysis causes the dissociation of C=Se bonds, giving rise to a high surface concentration of Se atoms. Ag_2Se layers are formed on the surface of Ag nanowires at 160°C and then growth of Ag_2Se layers is dominated by the outward diffusion of Ag^+ ions through the layer. The authors mentioned that the voids were observed to grow horizontally along the wire axis rather than isotropically because the adhesion of CSe_2 is preferred on the ends of the Ag nanowire rather than on its side faces. Hence, the high concentration of Se atoms at the nanowire ends promotes the diffusion of Ag^+ along the longitudinal axis, leading to the observed

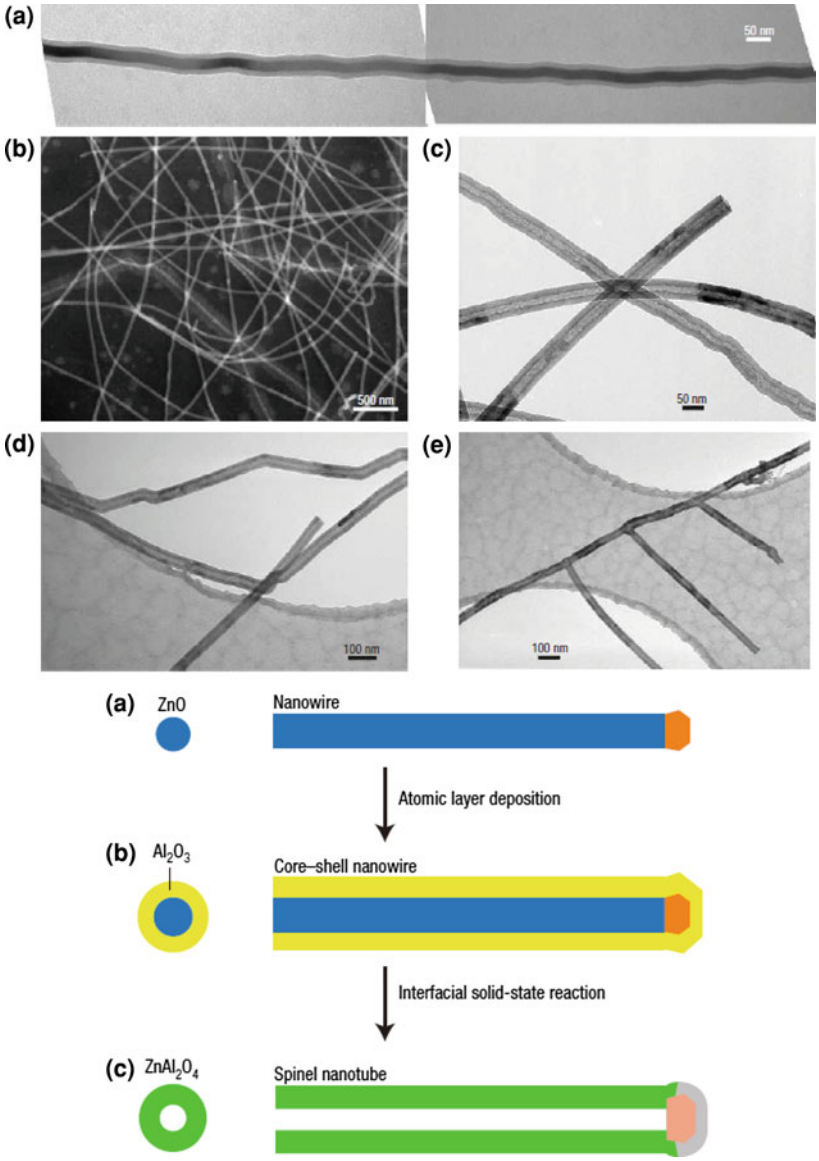

Fig. 11 Transformation of core–shell nanowires to nanotubes by means of the Kirkendall effect (*upper*). **a** TEM image of an example ZnO-Al_2O_3 core–shell nanowire. **b–e** Scanning electron microscopy (**b**) and TEM (**c–e**) images of $ZnAl_2O_4$ spinel nanotubes. Schematic diagram of the formation process of $ZnAl_2O_4$ spinel nanotubes (*lower*). **a** Single-crystal ZnO nanowires are grown by the vapor–liquid–solid mechanism using Au nanoparticles as a catalyst. **b** The nanowires are coated with a uniform layer of Al_2O_3 by ALD, forming core–shell ZnO–Al_2O_3 nanowires. **c** Annealing the core–shell nanowires leads to the formation of $ZnAl_2O_4$ nanotubes by a spinel-forming interfacial solid-state reaction involving the Kirkendall effect (reproduced with permission from [50])

anisotropic growth of vacancies along ⟨110⟩. This represents a different strategy of applying the Kirkendall effect to nanotube formation from the one presented in Fig. 11.

As mentioned in 2.2.1, the oxidation of metal nanoparticles is an effective route to fabricating hollow oxides because several metal nanoparticles such as Co, Cu, Fe, Zn, and Al turn into hollow oxide nanoparticles. It is expected, therefore, that the oxidation of such metal nanowires causes the formation of oxide nanotubes. Our latest results on the formation of oxide nanotubes through the oxidation of Fe, Cu and Ni nanowires [38] are introduced below.

Figure 13 shows the morphology changes of Fe, Cu and Ni nanowires before and after oxidation at 200–400°C. Voids were clearly observed along the interface

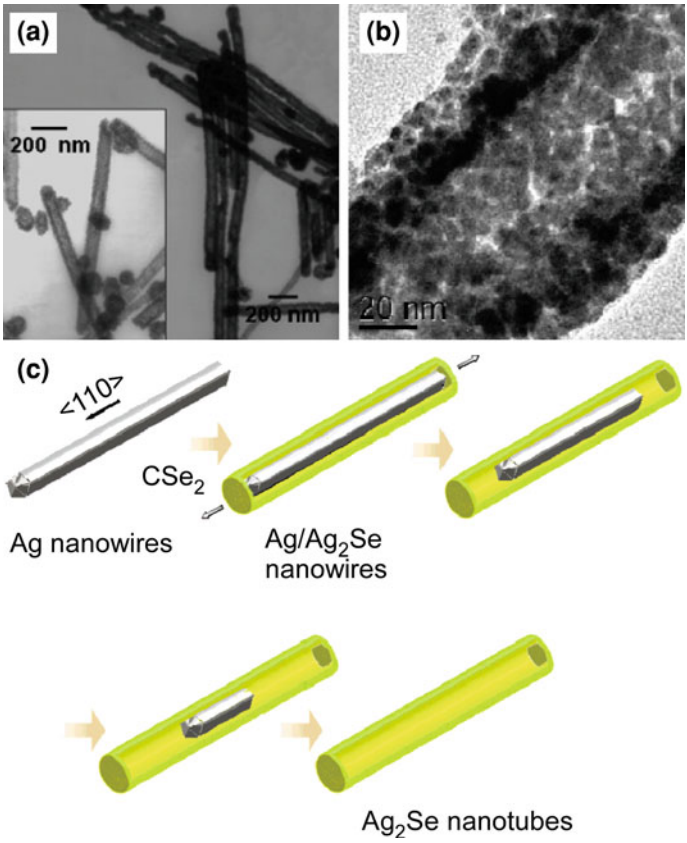

Fig. 12 Ag_2Se nanotubes formed based on the Kirkendall effect. **a** TEM image of the tubes. **b** Higher-magnification view of the tube showing that the tube wall is composed of multiple grains. **c** Schematic images of the diffusion process. Due to the higher concentration of CSe_2 adsorbed at the end (111) faces than on the side (100) faces of the Ag nanowires, the void grows along the longitudinal ⟨110⟩ direction from the ends. (Reproduced with permission from Ref. [28])

between the Fe nanowire and the outer oxide layer at 250°C for 3.6 ks. Finally, a Fe nanowire turned into a Fe_3O_4 (magnetite) nanotube with a cylindrical nanopore at 300°C for 3.6 ks. Similarly, interior voids with different sizes are fragmentarily generated inside the Cu nanowires after oxidation at 150°C for 1.2 ks. The oxidized Cu nanowires become nanotubes with a uniform inner and outer diameter at 150°C for 5.4 ks, as is the case with the oxidation of Fe nanowires. The crystal structure of the nanotubes obtained via the oxidation of the Cu nanowires at 150°C for 5.4 ks was identified to be Cu_2O. Cu_2O transformed into CuO at 300°C while maintaining the nanotube structure. In Fig. 13, representative electron micrographs of Ni nanowire after oxidation at 400 and 500°C are shown together. After oxidation at 400°C for 1.8 ks, large voids are formed at certain places at the interface between an inner remaining Ni wire and the outer oxide layer, as indicated by arrows. The formation behavior of voids at the interface between Ni and NiO is different from that between Fe and Fe_3O_4, where voids are uniformly formed along the interface. Ni nanowires became irregularly-shaped bamboo-like NiO with separate interior nanovoids of irregular diameters at 500°C for 3.6 ks.

The formation mechanism of Fe_3O_4 and Cu_2O nanotubes is illustrated in Fig. 14a; (1) an oxide layer is formed due to the oxidation reaction dominated by the outward diffusion of metal ions through the oxide layer, (2) voids are generated along the interface due to the inward diffusion of vacancies, which results from the Kirkendall effect, as the oxide layer grows, and (3) an oxide nanotube with a cylindrical pore is formed after all the metal atoms are consumed by reacting with oxygen. Fe_3O_4 and Cu_2O nanotubes obtained by oxidizing Fe and Cu nanowires have almost uniform inner and outer diameters, whereas NiO has separate interior voids and is irregular in shape. It can be expected that vacancies, which flow into the Ni side as a counter to the outward diffusion of Ni, migrate over a long-range distance, resulting in the growth of voids at certain places. A schematic illustration describing the void formation behavior during the oxidation of a Ni nanowire is shown in Fig. 14b. Vacancies, which are formed due to the outward diffusion of Ni at the interface between Ni and NiO, migrate toward a void (i). The growth of a localized void causes inhomogeneous oxide growth; the growth of the NiO layer is suppressed at the region with a void compared with the region without void in Ni (ii). As a result, a bamboo-like structure with separate interior voids and an irregular shape is formed (iii). As discussed in 2.2.1, both the localization of an interior void during the oxidation of Ni nanoparticles and nanowires seem to originate in the high mobility of vacancies in Ni during its oxidation.

3 Structural Stability of Hollow Nanostructures at High Temperatures

Thermal instability of hollow nanospheres was theoretically predicted by some groups [58–61]. Gusak et al. [59] proposed that vacancies flow outward from the

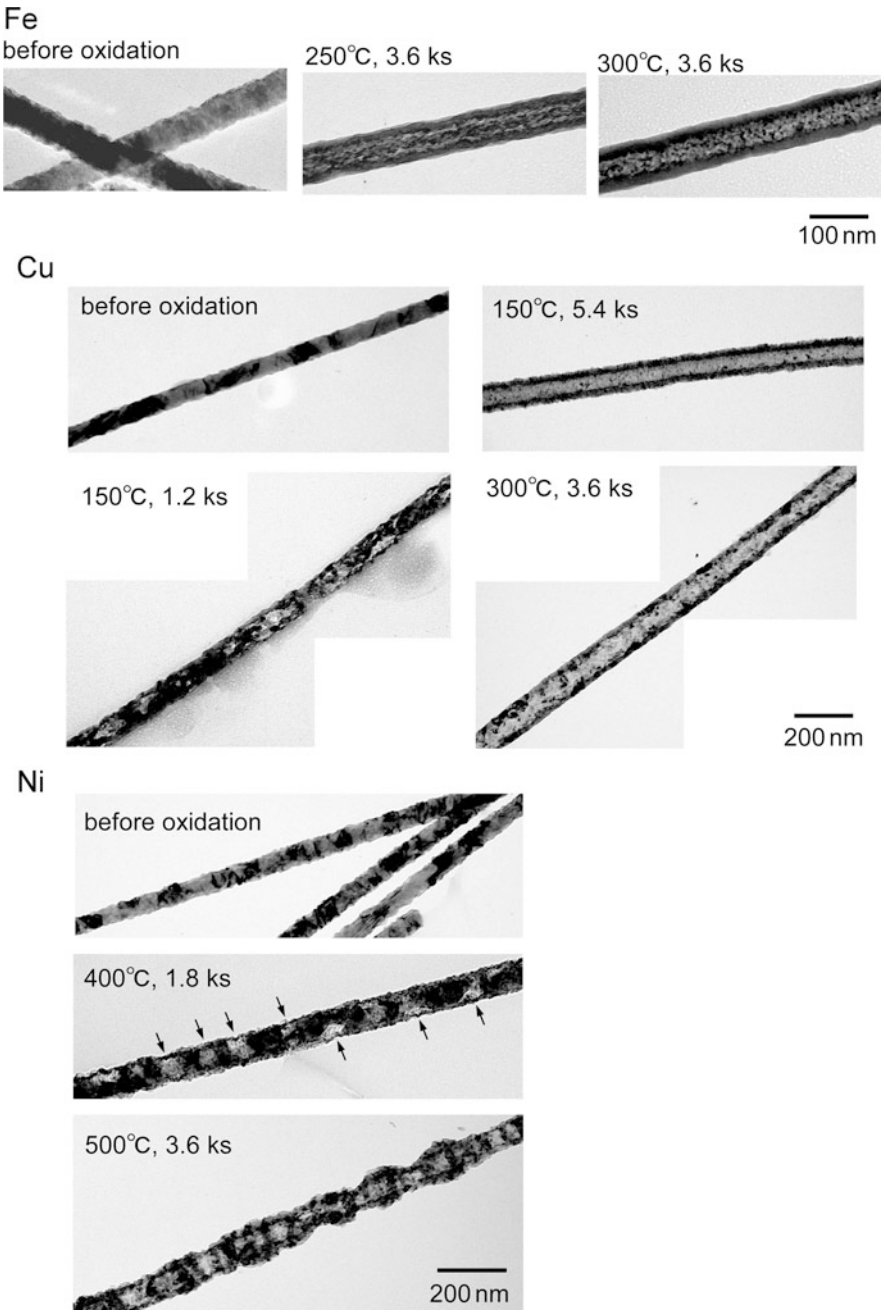

Fig. 13 TEM images of morphology change of Fe, Cu and Ni nanowires during oxidation (reproduced with permission from Ref. [38])

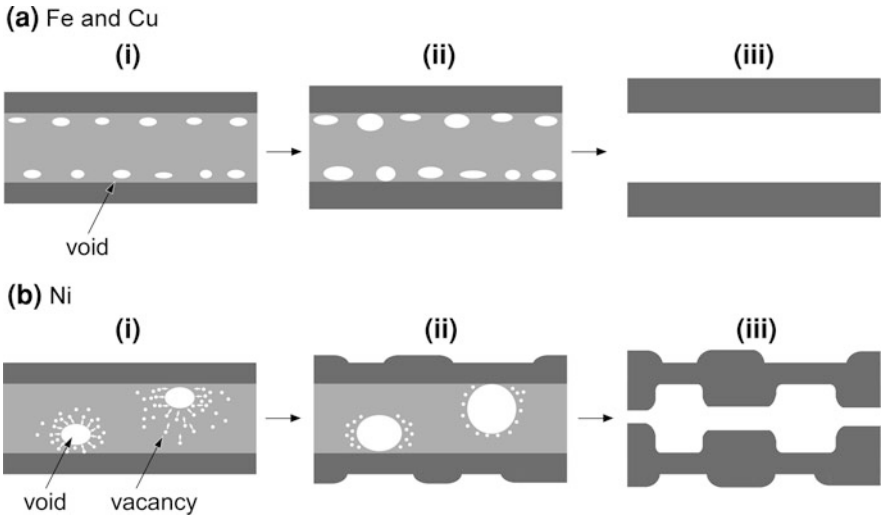

Fig. 14 Schematic illustration of morphological changes during oxidation of **a** Fe and Cu and **b** Ni: (*i*) formation of an oxide layer due to outward diffusion of metal ions through the initial oxide layer; (*ii*) formation of voids at the interface between the inner metal and outer oxide layer and (*iii*) formation of an oxide nanotube and bamboo-like structures with an interior nanopore (reproduced with permission from [38])

inner surface and absorbed at the outer surface since the vacancy concentration at the inner surface is higher than at the outer surface. As a result, the spheres shrink and finally end up eliminating the empty space to minimize the interface energy. According to their analysis, the rate of shrinking is controlled by the slow species in the case of a compound with a large difference between diffusivities of two components. On the other hand, experimental study on the stability of hollow nanostructures is limited to our reports [37, 38]. Shrinkage behavior of hollow oxide nanoparticles and nanotubes is reviewed in detail.

3.1 Shrinkage of Hollow Oxides

Figures 15a, b show changes in morphology of hollow Cu_2O and NiO nanoparticles during isochronal annealing under 4×10^{-5} Pa in a transmission electron microscope and their corresponding selected area electron diffraction (SAED) patterns [37]. The common characteristics are as follows: (i) hollow Cu_2O and NiO starts to shrink after annealing at a temperature where the reduction reactions from oxides to metals start, (ii) metal nanoparticles are formed at the inner surface of oxide shells, (iii) hollow oxides turn into metal nanoparticles without interior pores, and (iv) the changes in morphology and crystal structure through the

oxidation of metal nanoparticles and the reduction of hollow oxides can reversibly take place.

According to the kinetic models of reduction of oxides [62], oxygen ions are removed from the lattice of the surface leaving behind an anion vacancy and then

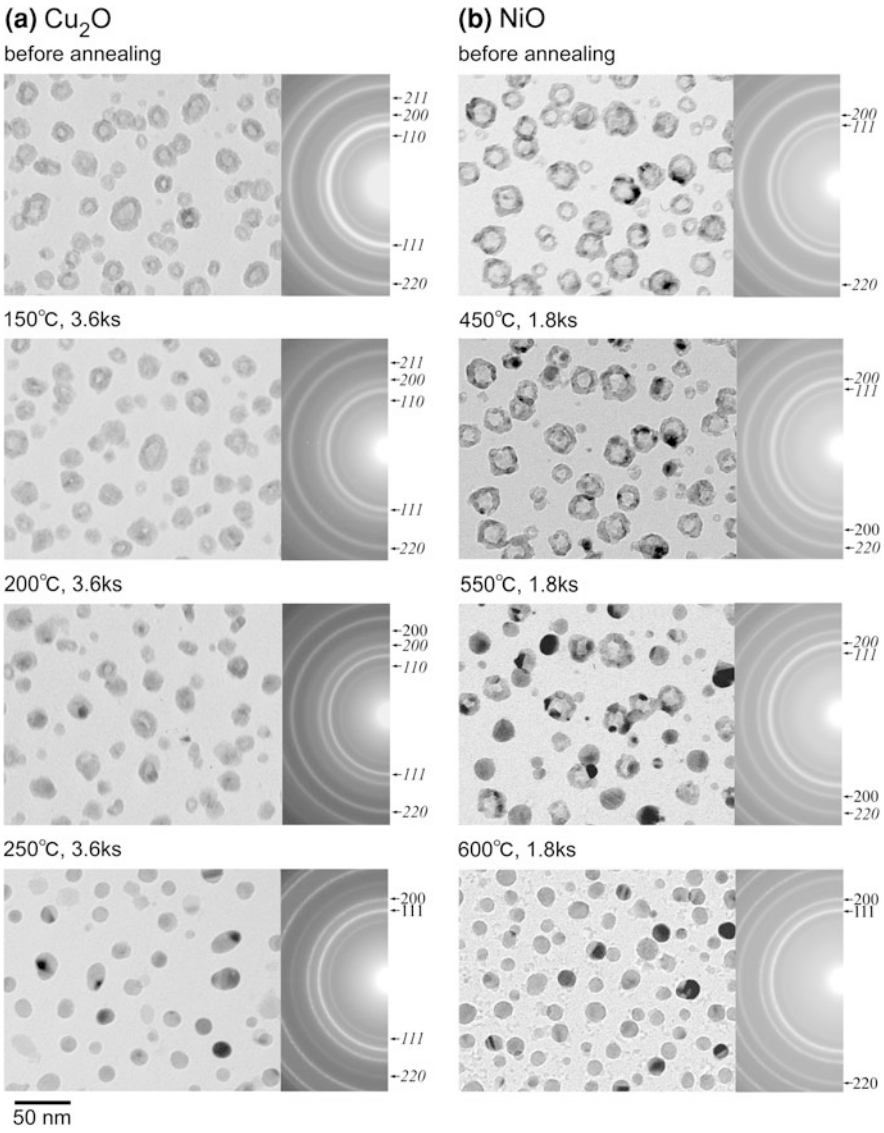

Fig. 15 Morphology changes of hollow Cu_2O and NiO nanoparticles before annealing and during isochronal annealing in TEM from 150 to 300°C. Initial diameters of hollow Cu_2O and NiO nanoparticles are 10–20 nm (reproduced with permission from [37])

reduced zone are formed on the surface at the initial stage of reduction. In general, a dominant process of reduction reaction is considered to be the outward diffusion of oxygen ions via the anion vacancies generated at the surface [62, 63]. Such mass transport results in the inward movement of the metal/reduced oxide interface. This is true of the reduction of hollow oxides; oxygen ions are removed from the outer surface to vacuum. As mentioned earlier, however, the formation of metal nanoparticles along the inner surface of hollow oxides during the reduction of Cu_2O to Cu and NiO to Ni, respectively, demonstrates that the reduced Cu and Ni atoms are generated at the inner surface of hollow Cu_2O and NiO. The formation of metal nanoparticles at the inner surface indicates that oxygen ions diffuse from the inner surface to the outer surface and that the reduced zone (i.e. Cu and Ni layers) is formed at the inner surface. After the formation of metal layers, metal atoms aggregate and make a particle in order to fill in the nano-hole. This behavior can be interpreted as the self-assembly of metal atoms which causes the extra energy of the inner surface of a hollow sphere to lower. The morphology change of hollow oxide nanoparticles annealed in reduction atmosphere is described in Fig. 16.

In the case of the annealing of hollow nanoparticles of CuO and NiO in air, shrinkage and collapse of hollow structures take place. Figures 17a, b show TEM images hollow CuO and NiO nanoparticles after annealing in air, respectively. The shrinkage of hollow CuO and NiO starts to occur at 400 and 650°C, respectively, and finally interior nanopores annihilate. CuO nanotubes and NiO bamboo-like (Fig. 13) structures also show a tendency to shrink and collapse through annealing at high temperatures, as shown in Fig. 18. It should be noted that the temperatures at which CuO nanotubes and NiO bamboo-like structures shrank are almost consistent with those for hollow nanoparticles of CuO and NiO.

According to the theoretical consideration on the shrinking of hollow binary alloy nanoparticles [59], the rate of shrinking is controlled by the slower diffusing species of the alloy. In fact, it was revealed that shrinking of both CuO and NiO by high-temperature oxidation starts at a temperature where the diffusion coefficient of the slower diffusion species reaches about 10^{-22} m^2s^{-1} [37].

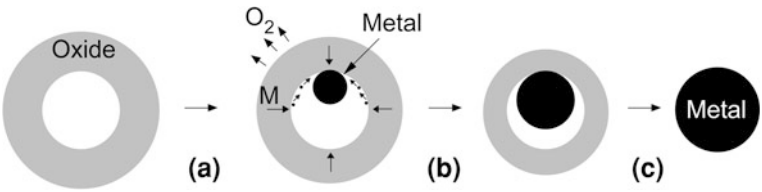

Fig. 16 Schematic illustration for morphology change of hollow oxide nanoparticles during annealing under reduction atmosphere: **a** desorption of oxygen from surface and the surface diffusion of reduced metal atoms at the inner surface, **b** growth of metal nanoparticles at the inner surface, and **c** formation of solid metal nanoparticles as a result of reduction of hollow oxides

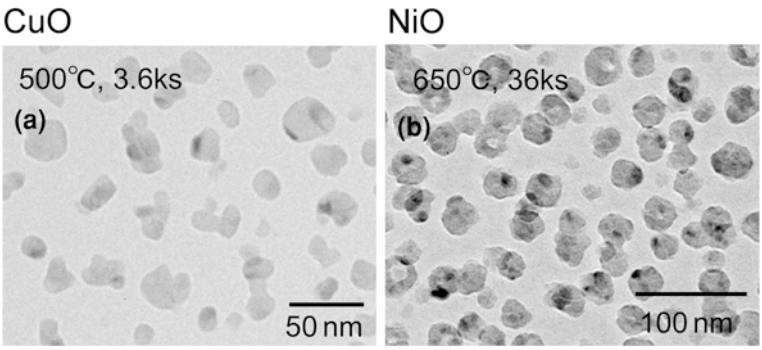

Fig. 17 CuO and NiO nanoparticles without interior nanopores after the annealing of hollow CuO and NiO at 500°C for 3.6 ks and 650°C for 36 ks, respectively (reproduced with permission from [37])

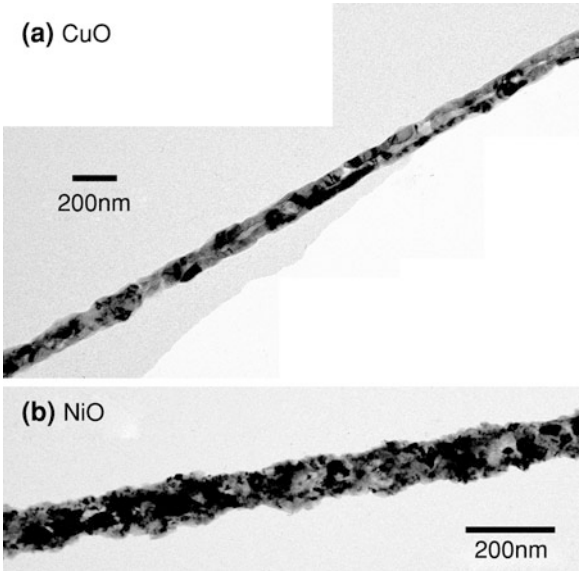

Fig. 18 TEM images of **a** CuO and **b** NiO nanotubes after annealing in air at 500°C for 3.6 ks and at 650°C for 3.6 ks, respectively (reproduced with permission from [38])

3.2 Transition in Porous Structures of Iron Oxides

Although hollow nanoparticles and nanotubes of Fe_3O_4 shrink and collapse by annealing at higher temperatures in air as is the case with Cu- and Ni-oxides, peculiar changes in morphology occur in the process from hollow structures to collapsed structures. In this section, the unique behavior is reviewed.

A typical example of the changes in the morphology after the oxidation of iron nanoparticles with the mean diameter of about 15 nm from 200 to 600°C is shown in Fig. 19. The morphology change from Fe nanoparticles to hollow Fe_3O_4 can be

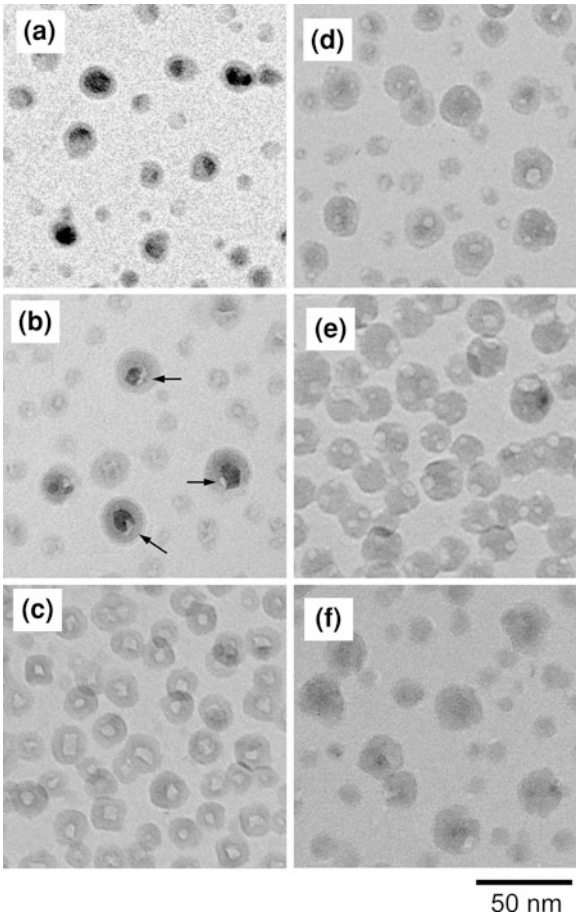

Fig. 19 A typical example of the morphology change of Fe nanoparticles (**a**) before and after oxidation at **b** 200°C for 18.0 ks, **c** 400°C for 90.0 ks, **d** 500°C for 3.6 ks, **e** 600°C for 3.6 ks and **f** 600°C for 14.4 ks (reproduced with permission from [44])

seen in Fig. 19a–c. After annealing at 500°C for 3.6 ks (Fig. 19d), two specific changes can be seen: (i) the nano-pores of the hollow particles become smaller and the location of nano-pores deviates from the center position, (ii) the additional smaller voids are generated in the particles; hollow nanoparticles with a single interior nano-pore turn into porous nanoparticles with a few voids by annealing the samples in air above 500°C. Furthermore, it was found that the interior closed pores became open surface pores at 600°C for 3.6 ks (Fig. 19e). Finally, porous iron oxide nanoparticles were observed to have turned into non-porous nanoparticles after the longer annealing time of 14.4 ks at 600°C, as shown in Fig. 19f.

Figure 20 shows representative electron micrographs of Fe_3O_4 nanotubes after annealing in air at 400 $\sim$ 600°C. As is the case with the oxidation of Fe nanoparticles, a further change in morphology can be seen after annealing at temperatures of 400°C and above; a number of voids with several nanometer sizes are formed along the inner side of the nanotube. These voids grow larger with increasing temperature. In addition, the duplex porous structures with a cylindrical

pore and a number of spherical pores transformed into porous structures without an inner cylindrical pore at 600°C for 3.6 ks, which was considered as a final form as a result of shrinkage. Above 673 K, both hollow nanoparticles and nanotubes of Fe_3O_4 transformed into γ-Fe_2O_3 [44].

The formation mechanism of hollow Fe_3O_4 nanoparticles and nanotubes via the oxidation of iron nanoparticles and nanowires below 400°C can be explained by a mechanism analogous to the Kirkendall effect in the Fe/oxide interface, where the outward diffusion of Fe is much faster than the inward diffusion of oxygen.

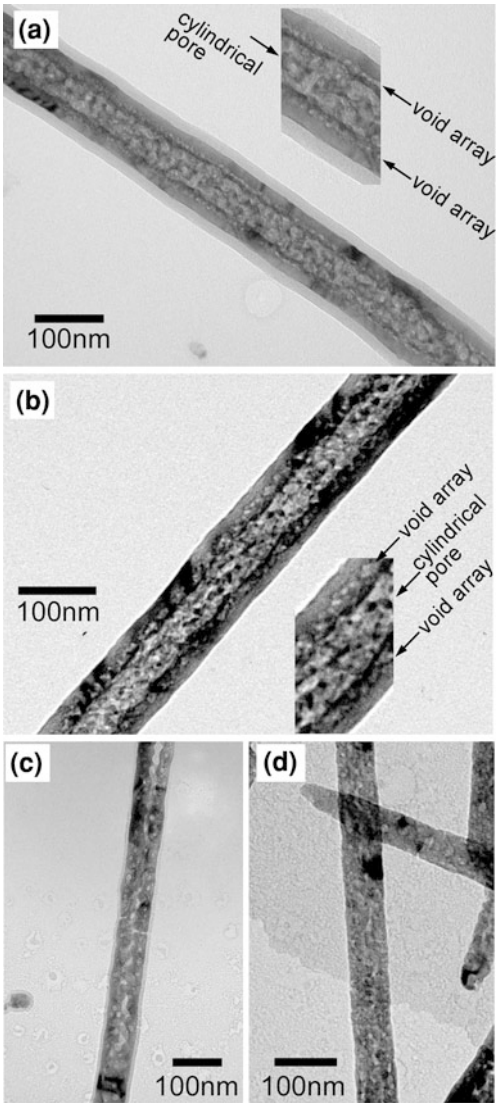

Fig. 20 A typical example of change in morphology of Fe_3O_4 nanotubes due to annealing in air: **a** 400°C, **b** 500°C and **c** 600°C for 3.6 ks. **d** The line profile of the corresponding diffraction patterns (reproduced with permission from [44])

The formation of an interior nano-pore inside an oxide particle and nanowire is due to the clustering of vacancies as a counter flow to the outward diffusion of iron ions.

It is noteworthy, however, that a peculiar change in morphology can be seen after annealing Fe_3O_4 hollow nanoparticles and nanotubes above 400°C in air; hollow structures with a single spherical and cylindrical nano-pore transform into porous structures with additional nano-voids. The morphology change from a hollow Fe_3O_4 nanoparticle and nanotube to porous structures is illustrated in Fig. 21; (i) vacancies diffuse outward from an interior pore as the pore shrinks, (ii) additionally spherical voids are introduced due to vacancy clustering, (iii) the shrinkage of the inner pore proceeds and the additional spherical voids grow larger, and (iv) γ-Fe_2O_3 nanoparticles and nanowires without nanopores were formed. This process is related to the phase transformation from Fe_3O_4 to γ-Fe_2O_3.

It is known that hollow nanostructures tend to shrink and collapse at high temperatures [37, 38]. As can be seen in Figs. 19 and 20, the interior pores of the hollow nanoparticles and nanotubes show a tendency to shrink and collapse. Therefore, the formation of additional nanovoids is associated with the annihilation of the interior nanopores in hollow nanoparticles and nanotubes. According to Gusak et al. [59], the shrinkage of hollow nanoparticles can be described as the outward diffusion of vacancies from the inner pores (vacancy source) to the surface (vacancy sink) of hollow nanoparticles. It is possible, therefore, to speculate that the vacancies, which generate from an inner pore, diffuse outward and then contribute to the formation of additional nanovoids. Furthermore, the phase transformation from Fe_3O_4 to γ-Fe_2O_3 occurs in the shrinkage process. Thus, the formation of additional nano-voids during the annealing of hollow Fe_3O_4 in air at

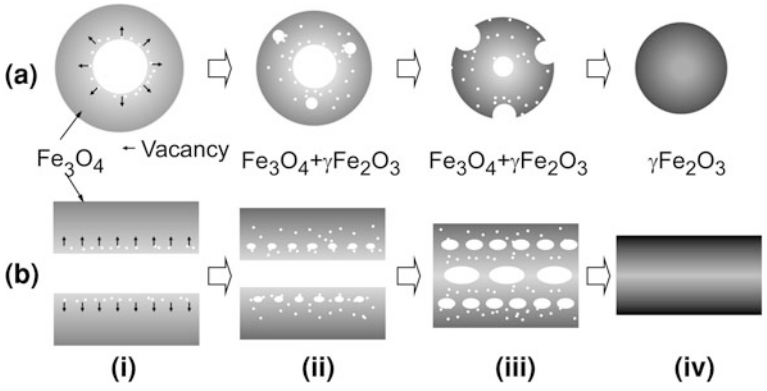

Fig. 21 Schematic illustrations of transition in the morphology of a Fe_3O_4: **a** hollow nanoparticle and **b** nanotube: (*i*) dissociation of vacancies at the inner surface of a hollow nanoparticle and nanotubes of Fe_3O_4; (*ii*) formation of additional spherical voids associated with shrinkage of an internal pore and phase transformation from Fe_3O_4 to γ-Fe_2O_3; (*iii*) growth of voids and shrinkage of an interior pore; and (*iv*) the formation of non-porous γ-Fe_2O_3.Vacancies are generated from inner surface and diffuse outward. The outward vacancy diffusion accompanies the phase transformation from Fe_3O_4 to γ-Fe_2O_3. The vacancies combine to form voids during the diffusion process (reproduced with permission from [44])

high temperatures is closely related to the phase transformation from Fe_3O_4 and γ-Fe_2O_3. The possible formation mechanism of additional nanovoids is the recombination of the out-going vacancies in the vicinity of the interface between Fe_3O_4 and γ-Fe_2O_3, which may result in the relaxation of interface strain. The details are given in Ref. [44].

Formation of hollow nanostructures by the Kirkendall effect is induced by the inward diffusion of excess vacancies during solid-state reactions. On the other hand, shrinkage behavior of hollow nanostructures is closely related to outward diffusion of vacancies from interior nanopores. Therefore, not only the inward but also the outward migration of vacancies may give rise to changes in morphology in the case of porous structures at elevated temperatures.

4 Summary

In the past few years, there have been considerable advancements concerning the synthesis of hollow nanoparticles and nanotubes. The synthesis routes based on chemical reactions such as chemical etching and galvanic replacement are broadly used for a wide variety of materials. More information on the chemical synthesis routes can be obtained in references [4] and [5]. In addition, different ideas have been applied to the fabrication of hollow nanomaterials. For example, the Kirkendall-effect-related processes have been recognized as one of the useful methods for the fabrication of oxides, sulfides and phosphides. Since the Kirkendall effect is related to the mass transport at the interface between different solids, there is much possibility to control hollow nanostructures of a variety of alloys and intermetallic compounds. The result by Fan et al., who successfully fabricated $ZnAl_2O_4$ spinel nanotubes from ZnO/Al_2O_3 core/shell nanowires, strongly suggests the formation of A–B alloys or compounds if A/B core/shell type nanostructures are easily obtained.

Our recent studies on the shrinkage behavior of hollow nanoparticles and nanotubes are also introduced. Hollow nanoparticles and nanotubes of metal oxides tend to shrink and collapse at higher temperatures both in reduction and oxidation atmosphere because hollow nanostructures with an inner surface are energetically unstable. The shrinking of hollow oxides occurs at temperatures where the reduction reactions from oxides to metals start in annealing them in reduction atmosphere. Hollow oxides turn into solid metal nanoparticles as a result of the shrinking associated with reduction. On the other hand, shrinking of hollow oxides occurs at temperatures where the diffusion coefficients of slower diffusing ions in the oxides are of the order of 10^{-22} m^2 s^{-1}. These results suggest that it is possible to control the size of interior nanopores and particles using annealing in high temperatures. In the case of hollow iron oxide, however, a peculiar morphology change is induced in the process of shrinkage; hollow oxides with an interior spherical and cylindrical nanopore transform into porous structures with additional multiple nanovoids. Transition in porous structure seems to be related to

the outward diffusion of vacancies from interior pore and the phase transition from magnetite to maghemite. It was found by our experiments that the outward diffusion of vacancies that takes place during shrinkage contribute to the formation of a unique nanoporous structure. It should be pointed out that annealing of hollow nanostructures at high temperatures may induce further change in morphology in some cases. Further research works should be carried out to investigate the performance of different nanostructures at high temperature.

References

1. Xia, Y., Halas, N.J.: Shape-controlled synthesis and surface plasmonic properties of metallic nanostructures. MRS Bull **30**, 338–343 (2005)
2. Xia, Y., Yang, P., Sun, Y., et al.: One-dimensional nanostructures: synthesis, characterization, and applications. Adv. Mater. **15**, 353–389 (2003)
3. Fan, H.J., Göele, U., Zacharias, M.: Formation of nanotubes and hollow nanoparticles based on Kirkendall and diffusion processes: a review. Small **3**, 1660–1671 (2007)
4. Lou, X.W., Archer, L.A., Yang, Z.: Hollow micro-/nanostructures: synthesis and applications. Adv. Mater. **20**, 3987–4019 (2008)
5. An, K., Hyeon, T.: Synthesis and biomedical applications of hollow nanostructures. Nano. Today **4**, 359–373 (2009)
6. Smigelskas, A.D., Kirkendall, E.O.: Zinc diffusion in alpha brass. Trans. AIME **171**, 130–142 (1947)
7. Ostwald, W.: On the assumed isomerism of red and yellow mercury oxide and the surface-tension of solid bodies. Z. Phys. Chem. **34**, 495 (1900)
8. Yin, Y., Rioux, R.M., Erdonmez, C.K., et al.: Formation of hollow nanocrystals through the nanoscale Kirkendall effect. Science **304**, 711–714 (2004)
9. Caruso, F., Caruso, R.A., Mohwald, H.: Nanoengineering of inorganic and hybrid hollow spheres by colloidal templating. Science **282**, 1111–1114 (1998)
10. Kim, S.-W., Kim, M., Lee, W.Y., et al.: Fabrication of hollow palladium spheres and their successful application to the recyclable heterogeneous catalyst for Suzuki coupling reactions. J. Am. Chem. Soc. **124**, 7642–7643 (2002)
11. Caruso, F., Shi, X., Caruso, R.A., et al.: Hollow titania spheres from layered precursor deposition on sacrificial colloidal core particles. Adv. Mater. **13**, 740–744 (2001)
12. Chen, G.-C., Kuo, C.-Y., Lu, S.-Y.: A general process for preparation of core-shell particles of complete and smooth shells. J. Am. Ceram. Soc. **88**, 277–283 (2005)
13. Martinez, C.J., Hockey, B., Montgomery, C.B., et al.: Porous tin oxide nano-structured microspheres for sensor applications. Langmuir **21**, 7937–7944 (2005)
14. Liang, Z., Susha, A., Caruso, F.: Gold nanoparticles-based core/shell and hollow spheres and ordered assemblies thereof. Chem. Mater. **15**, 3176–3183 (2003)
15. Caruso, F., Spasova, M., Susha, A., et al.: Magnetic nanocomposite particles and hollow spheres constructed by a sequential layering approach. Chem. Mater. **13**, 109–116 (2000)
16. Goldberger, J., He, R., Zhang, Y., et al.: Single-crystal gallium nitride nano-tubes. Nature **422**, 599–602 (2003)
17. Shen, G., Bando, Y., Ye, C., et al.: Single-crystal nanotubes of II_3–V_2 semi-conductors. Angew. Chem. Int. Ed. **45**, 7568–7572 (2006)
18. Ras, R.H.A., Kemell, M., Wit, J., et al.: Hollow inorganic nanospheres and nanotubes with tunable wall thicknesses by atomic layer deposition on self-assembled polymeric templates. Adv. Mater. **19**:102–106 (2007)
19. Schmidt, O.G., Eberl, K.: Nanotechnology: thin solid films roll up into nanotubes. Nature **410**, 168 (2001)

20. Schmidt, O.G., Schmarje, N., Deneke, C., et al.: Three-dimensional nano-objects evolving from a two-dimensional layer technology. Adv. Mater. **13**, 756–759 (2001)
21. Sun, Y., Mayers, B.T., Xia, Y.: Template-engaged replacement reaction: a one-step approach to the large-scale synthesis of metal nanostructures with hollow interiors. Nano. Lett. **2**, 481–485 (2002)
22. Chen, J., Wiley, B., McLellan, J., et al.: Optical properties of Pd/Ag and Pt/Ag nanoboxes synthesized via galvanic replacement reactions. Nano. Lett. **5**, 2058–2062 (2005)
23. Sun, Y., Xia, Y.: Mechanistic study on the replacement reaction between silver nanostructures and chloroauric acid in aqueous medium. J. Am. Chem. Soc. **126**, 3892–3901 (2004)
24. Lou, X.W., Wang, Y., Yuan, C., et al.: Template-free synthesis of SnO_2 hollow nanostructures with high lithium storage capacity. Adv. Mater. **18**, 2325–2329 (2006)
25. Yang, H.G., Zeng, H.C.: Creation of intestine-like interior space for metal-oxide nanostructures with a quasi-reverse emulsion. Angew. Chem. Int. Ed. **43**, 5206–5209 (2004)
26. Teo, J.J., Chang, Y., Zeng, H.C.: Fabrications of hollow nanocubes of Cu_2O and Cu via reductive self-assembly of CuO nanocrystals. Langmuir **22**, 7369–7377 (2006)
27. Liu, B., Zeng, H.C.: Symmetric and asymmetric Ostwald ripening in the fabrication of homogeneous core-shell semiconductors. Small **1**, 566–571 (2005)
28. Bernard Ng, C.H., Tan, H., Fan, W.Y.: Formation of Ag_2Se nanotubes and dendrite-like structures from UV irradiation of a CSe_2/Ag colloidal solution. Langmuir **22**, 9712–9717 (2006)
29. Ma, Y., Huo, K., Wu, Q., et al.: Self-templated synthesis of polycrystalline hollow aluminium nitride nanospheres. J. Mater. Chem. **16**, 2834–2838 (2006)
30. Zheng, J., Song, X., Zhang, Y., et al.: Nanosized aluminum nitride hollow spheres formed through a self-templating solid-gas interface reaction. J. Solid State Chem. **180**, 276–283 (2007)
31. Nakamura, R., Tokozakura, D., Nakajima, H., et al.: Hollow oxide formation by oxidation of Al and Cu nanoparticles. J. Appl. Phys. **101**, 074303 (2007)
32. Li, Q., Penner, R.M.: Photoconductive cadmium sulfide hemicylindrical shell nanowire ensembles. Nano. Lett. **5**,1720–1725 (2005)
33. Li, Y., Tan, B., Wu, Y.: Freestanding mesoporous quasi-single-crystalline Co_3O_4 nanowire arrays. J. Am. Chem. Soc. **128**, 14258–14259 (2006)
34. Chen, X., Zhang, Z., Qiu, Z., et al.: Hydrothermal fabrication and characterization of polycrystalline linneite (Co_3S_4) nanotubes based on the Kirkendall effect. J. Colloid Interface Sci. **308**, 271–275 (2007)
35. Gao, J., Zhang, B., Zhang, X., et al.: Magnetic-dipolar-interaction-induced self-assembly affords wires of hollow nanocrystals of cobalt selenide. Angew. Chem. Int. Ed. **45**, 1220–1223 (2006)
36. Chou, N.H., Schaak, R.E.: A library of single-crystal metal-tin nanorods: using diffusion as a tool for controlling the morphology of intermetallic nanocrystals. Chem. Mater. **20**, 2081–2085 (2008)
37. Nakamura, R., Tokozakura, D., Lee, J.G., et al.: Shrinking of hollow Cu_2O and NiO nanoparticles at high temperatures. Acta Mater. **56**, 5276–5284 (2008)
38. Nakamura, R., Matsubayashi, G., Tsuchiya, H., et al.: Formation of oxide nanotubes via oxidation of Fe, Cu and Ni nanowires and their structural stability: difference in formation and shrinkage behavior of interior pores. Acta Mater. **57**, 5046–5052 (2009)
39. Wang, Q., Li, J.-X., Li, G.-D., et al.: Formation of CuS nanotube arrays from CuCl nanorods through a gas-solid reaction route. J. Cryst. Growth **299**, 386–392 (2007)
40. Cao, H., Qian, X., Wang, C., et al.: High symmetric 18-facet polyhedron nanocrystals of Cu_7S_4 with a hollow nanocage. J Am Chem Soc **127**, 16024–16025 (2005)
41. Wang, C.M., Baer, D.R., Thomas, L.E., et al.: Void formation during early stages of passivation: Initial oxidation of iron nanoparticles at room temperature. J. Appl. Phys. **98**, 094307–094308 (2005)
42. Cabot, A., Puntes, V.F., Shevchenko, E., et al.: Vacancy coalescence during oxidation of iron nanoparticles. J. Am. Chem. Soc. **129**, 10358–10360 (2007)

43. Peng, S., Sun, S.: Synthesis and characterization of monodisperse hollow Fe_3O_4 nanoparticles. Angew. Chem. Int. Ed. **46**, 4155–4158 (2007)
44. Nakamura, R., Matsubayashi, G., Tsuchiya, H., et al.: Transition in nanoporous structure of iron oxides during the oxidation of iron nanoparticles and nanowires. Acta Mater. **57**, 4261–4266 (2009)
45. Ye, L., Wu, C., Guo, W., et al.: MoS_2 hierarchical hollow cubic cages assembled by bilayers: one-step synthesis and their electrochemical hydrogen storage properties. Chem. Commun. 4738–4740 (2006)
46. Nakamura, R., Lee, J.G., Mori, H., et al.: Oxidation behaviour of Ni nanoparticles and formation process of hollow NiO. Philos. Mag. **88**, 257–264 (2008)
47. Chiang, R.-K., Chiang, R.-T.: Formation of hollow Ni_2P nanoparticles based on the nanoscale Kirkendall effect. Inorg. Chem. **46**, 369–371 (2006)
48. Gaiduk, P.I., Hansen, J.L., Larsen, A.N.: Synthesis and analysis of hollow SnO_2 nanoislands. Appl. Phys. Lett. **92**, 193112 (2008)
49. Wang, Y., Cai, L., Xia, Y.: Monodisperse spherical colloids of Pb and their use as chemical templates to produce hollow particles. Adv. Mater. **17**, 473–477 (2005)
50. Fan, H.J., Knez, M., Scholz, R., et al.: Monocrystalline spinel nanotube fabrication based on the Kirkendall effect. Nat. Mater. **5**, 627–631 (2006)
51. Fan, H.J., Knez, M., Scholz, R., et al.: Influence of surface diffusion on the formation of hollow nanostructures induced by the Kirkendall effect: the basic concept. Nano. Lett. **7**, 993–997 (2007)
52. Fan, H.J., Scholz, R., Kolb, F.M., et al.: Growth mechanism and characterization of zinc oxide microcages. Solid State Commun. **130**, 517–521 (2004)
53. Liu, B., Zeng, H.C.: Fabrication of ZnO dandelions via a modified Kirkendall process. J. Am. Chem. Soc. **126**, 16744–16746 (2004)
54. Nakamura, R., Lee, J.G., Tokozakura, D., et al.: Formation of hollow ZnO through low-temperature oxidation of Zn nanoparticles. Mater. Lett. **61**, 1060–1063 (2007)
55. Lu, H.B., Li, H., Liao, L., et al.: Low-temperature synthesis and photocatalytic properties of ZnO nanotubes by thermal oxidation of Zn nanowires. Nanotechnology **19**, 045605 (2008)
56. Zhou, J., Liu, J., Wang, X., et al.: Vertically aligned Zn_2SiO_4 nanotube/ZnO nanowire heterojunction arrays. Small **3**, 622–626 (2007)
57. Tokozakura, D., Nakamura, R., Nakajima, H., et al.: Transmission electron microscopy observation of oxide layer growth on Cu nanoparticles and formation process of hollow oxide particles. J. Mater. Res. **22**, 2930–2935 (2007)
58. Tu, K.N., Gösele, U.: Hollow nanostructures based on the Kirkendall effect: design and stability considerations. Appl. Phys. Lett. **86**, 093111 (2005)
59. Gusak, A.M., Zaporozhets, T.V., Tu, K.N., et al.: Kinetic analysis of the instability of hollow nanoparticles. Philos. Mag. **85**, 4445–4464 (2005)
60. Evteev, A.V., Levchenko, E.V., Belova, I.V., et al.: Shrinking kinetics by vacancy diffusion of a pure element hollow nanosphere. Philos. Mag. **87**, 3787–3796 (2007)
61. Fischer, F.D., Svoboda, J.: High temperature instability of hollow nanoparticles. J. Nanoparticle Res. **10**, :255–261 (2008)
62. Kung, H.H.: Transition Metal Oxides: Surface Chemistry and Catalysis. Elsevier, New York (1989)
63. Scholz, J.J., Langell, M.A.: Kinetic analysis of surface reduction in transition metal oxide single crystals. Surf. Sci. **164**, 543–557 (1985)